IEEE Photonics Journal
An IEEE Photonics Society Publication

Open Access

Modified All-Fiber Fabry–Perot Interferometer and Its Refractive Index, Load, and Temperature Analyses

Volume 7, Number 3, June 2015

D. Jauregui-Vazquez
Y. Lopez-Dieguez
J. M. Sierra-Hernandez
M. Perez-Maciel
M. S. Avila-Garcia
E. Vargas-Rodriguez
R. Rojas-Laguna
J. M. Estudillo-Ayala

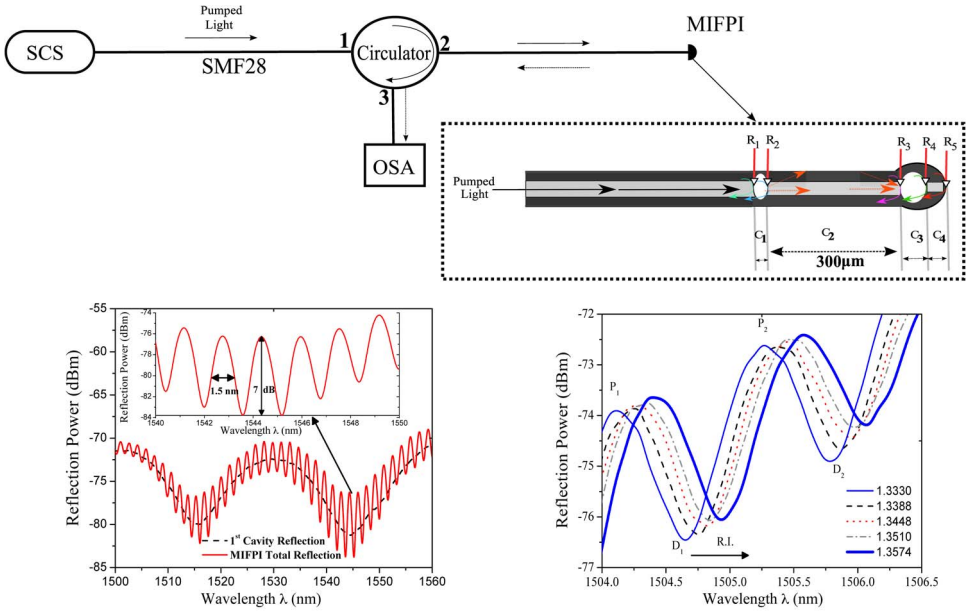

DOI: 10.1109/JPHOT.2015.2437374
1943-0655 © 2015 IEEE

IEEE photonics SOCIETY

IEEE

Modified All-Fiber Fabry–Perot Interferometer and Its Refractive Index, Load, and Temperature Analyses

D. Jauregui-Vazquez,[1] Y. Lopez-Dieguez,[1] J. M. Sierra-Hernandez,[2] M. Perez-Maciel,[1] M. S. Avila-Garcia,[2] E. Vargas-Rodriguez,[2] R. Rojas-Laguna,[1] and J. M. Estudillo-Ayala[1]

[1]Departamento de Electrónica, División de Ingenierías Campus Irapuato-Salamanca, Universidad de Guanajuato, 36885 Salamanca, Gto., Mexico
[2]Departamento de Estudios Multidisciplinarios, División de Ingenierías Campus Irapuato-Salamanca, Universidad de Guanajuato, 38940 Yuriria, Gto., Mexico

DOI: 10.1109/JPHOT.2015.2437374

Manuscript received April 23, 2015; revised May 15, 2015; accepted May 20, 2015. Date of current version June 15, 2015. This work was supported in part by CONACYT under Repatriation Program 243981 and UG-DAIP 436/2014. The work of D. Jauregui-Vazquez was supported by CONACYT under student scholarship 290549/226889. Corresponding author: J. M. Estudillo-Ayala (e-mail: julian@ugto.mx).

Abstract: An all-fiber Fabry–Perot (FP) interferometer is proposed and validated by the arc splicing technique. By using conventional fiber and special hollow-core photonic crystal fiber, several FP cavities were formed at the conventional fiber tip using arc discharges. As a result of the interaction between these cavities, modified FP principle operation was obtained; and temperature, refractive index, and load analyses validated this operation modification. In addition, this all-fiber interferometer presents good resolution and sensitivity in each parameter examined. The structure offers compactness, robustness, high repeatability, and stability measurement.

Index Terms: Fiber optics systems, sensors, fabrication and characterization.

1. Introduction

Over the past few years, researchers have been paying attention to a new all-fiber Fabry–Perot interferometers technique fabrication [1], driven by the interest to improve its sensibility, resolution, and stability. As a result, several fabrication techniques have been proposed, and their sensing applications, such as temperature [2], [3], refractive index [2], [4], [5], curvature [6], magnetic field [7], strain [3], [8], load [9], pressure [10], etc, have been demonstrated. Some prior works propose using a high power pulse laser to create a micro machined FP cavity at the tip of conventional single mode fiber (SMF28) to detect refractive index changes, and these experiments show is possible to obtain a high resolution using this FP structure; however, the fabrication cost increase by the kind of laser used [4]. In other letters [8], [10]–[13], a technique to obtain a splice joint between SMF28 and different types of special fiber such as: hollow core fibers, hollow core photonic crystal fibers or capillary fibers was proposed, here several parameters analyses validated the use of this all fiber Fabry–Perot interferometers in sensing applications; nevertheless, special splicers, as well as complex procedures, are required to obtain the sensing device. One of the techniques that reduce the cost, consist on use an arc splicer and SMF28 fiber, in these works by re-shaping the conventional fiber tip or using a special

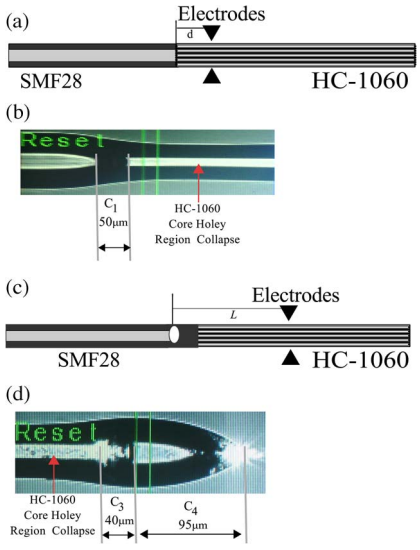

Fig. 1. Fabrication of a MIFPI. (a) Initial position using the splice joint SMF28-HC-1060. (b) Splicer image from the first air cavity (C_1) formed. (c) Drawing of HC-1060 position to generated C_3 and C_4. (d) Illuminated MIFPI tip view by visible light.

technique a FP cavity is generated applying several arc discharges, as a result, an in-line FP cavity was formed and used to monitoring simultaneous parameters measurements [8], [14]. In this work, splicing and cleaving are used to generate a Modified Intrinsic Fabry–Perot Interferometer (MIFPI), as a result versatile technique is demonstrated. The structure presents a modified response than conventional FP cavities and discussion is carry out, moreover to prove potential applications: refractive index, load, and temperature response were analyzed.

2. MIFPI Fabrication Process and Principle of Operation

2.1. Fabrication Device

In order to generate our MIFPI, conventional single mode fiber (SMF28) and special hollow core photonic crystal fiber (HC-1060) were used. These fibers were cleaved and set into Fitel S175 fusion splicer and then using the parameters and procedure proposed by [15], a splice joint SMF28-HC-1060 was obtained. Afterward, using the splicer manual mode, the splice joint was translated a distance ($d = 50\ \mu m$) from the electrodes [see Fig. 1(a)]. At this point the parameters in Table 1 were assigned and three discharges were applied, as a result an air cavity (C_1) was formed as can be appreciated in Fig. 1(b).

The next step consists of placing C_1 a distance $L = 550\ \mu m$ from the electrodes [see Fig. 1(c)] and using the same parameters in Table 1, several discharges were applied until the HC-1060 was separated into two parts and forming C_3 and C_4 at the SMF28 tip as can be appreciated in Fig. 1(d). As a consequence, to applied the discharges all the HC-1060 core holey region structure (50 μm) collapse forming a solid material [see white region in Fig. 1(b)], and the solid cladding region in the HC-1060 fiber remains without changes. Here a new structure is formed and composed by a sort of solid core (holey structure region collapse) and a sort of cladding (HC-1060 cladding region), this structure provide two different optical paths and form a cavity C_2 in the MIFPI structure between C_1 and C_3. The structure of the MIFPI can be appreciated on the bottom right inset of Fig. 2.

2.2. MIFPI Characterization

To characterize the MIFPI, the experimental setup from Fig. 2 was implemented, here, the pumped light from the supercontinuum source (SCS) proposed by [16], goes to the fiber optic

TABLE 1

Assigned parameters

Parameter	Value
Power	94
Pre-fusion Time (ms)	50
Arc Duration (ms g)	50
Cleaning Time (ms)	0

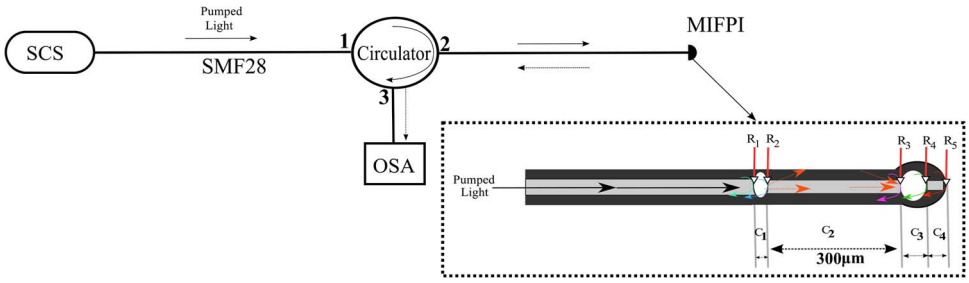

Fig. 2. Experimental setup to characterized MIFPI. (Bottom right inset) Schematic MIFPI diagram.

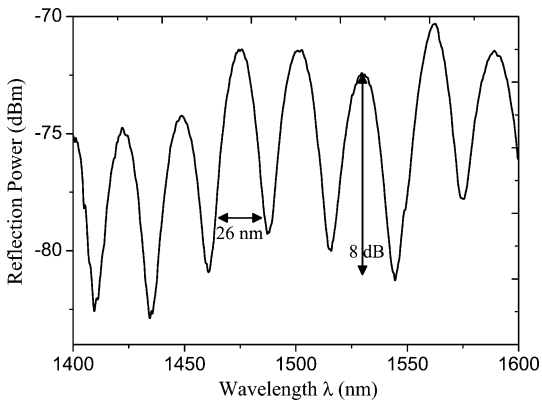

Fig. 3. Interference spectrum generated by C_1.

circulator and pass until reaching the MIFPI, the reflection provided by this one is analyzed by an Optical Spectrum Analyzer (OSA).

Multiples Fabry–Perot (FP) cavities into the MIFPI are formed by the boundaries between silica and air interface and each FP cavity is formed by low reflections $(\approx 4\%)$ which will be analyzed. The first reflections occur when the pumped light that travels into the SMF28 $(n_s = 1.4681)$ arrive to the C_1 $(n_a = 1.00)$ and a refractive index change occur, as a result of the silica-air interface, one part of the light is transmitted and the rest is reflected generating reflection R_1, the light that continue into C_1, reaches at the end of the cavity and the same refractive index change $(n_a - n_s)$ occur, here reflection (R_2) is generated. These reflections (R_1 and R_2) provide a Fabry–Perot (FP) cavity and generate an interference spectrum that is showed in Fig. 3; this spectrum was obtained during the fabrication process. Using the Free Spectral Range (FSR) relation: $\Delta\lambda = \lambda^2/2nd$ is possible to estimated the cavity distance, here λ is the wavelength of the light

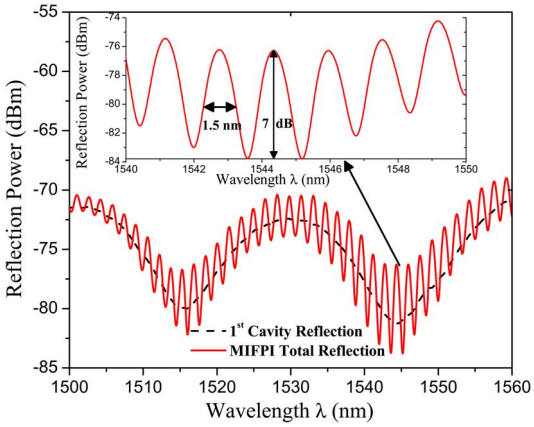

Fig. 4. Interference spectrum span generated by MIFPI.

in the cavity, n is the refractive index of the cavity, and d is the cavity distance; by the analysis of Fig. 3: $\Delta\lambda = 26$ nm, $\lambda = 1530$ nm and $n_a = 1.00$. The C_1 distance obtained is around 45 μm; in contrast to the values estimated using the arc splicer, an error around 5 μm exits, this error has to do with the losses and irregular shape of the cavity.

The next reflections occur when the light transmitted by C_1 travels to the end of C_2, however at the C_2 initial point the light is spread out in two different optical paths, due to C_2 is composed by a sort of core and cladding, formed by the HC-1060 structure collapse, as a consequence an interference is generated when this two different optical paths delays are coupling at the end of C_2. As a result, reflection R_3 is generated at the end of C_2 by the presence of an air cavity, the rest of the light provided by C_1 and C_2 continue traveling by C_3 at the end of this cavity reflection R_4 is generated, then the rest of the light transmitted goes through the last silica cavity (C_4) and the last two reflections (R_4 and R_5) are generated in this point; all these reflections generate a MIFPI total interference spectrum; from, Fig. 3, a specific fringe spectrum was chosen to show the MIFPI interference in Fig. 4.

In Fig. 4 the MIFPI interference is envelope over C_1 reflection spectrum, here different frequencies can appreciated due to the contribution from the others cavities interference (C_2, C_3 and C_4). As can be appreciated in the middle inset of Fig. 4 the MIFPI interference has a FSR $= 1.5$ nm and a visibility oscillation as a consequence of the cavity losses for specific wavelengths. Several MIFPI were fabricated using the process described above and the cavities distance estimated using the arc splicer were similar for each MIFPI. These values are showed in Figs. 1 and 2.

2.3. Principle of Operation of the MIFPI

The interference spectrum generated by the MIFPI for specific span is showed into inset Fig. 5. When we applied the Fast Fourier Transform (FFT) to the interference spectrum inset, fiber modes contribution can be analyzed. As can be appreciated in Fig. 5, several modes are involved to generate the interference spectrum; these modes were produced by the cavities described above.

Usually, in FP spatial frequency analysis, the peak represents the contribution of the cavities involve. However in this case, C_2 generate an interference between two modes, as a result of the two different optical paths provided by the cavity structure; as a consequence the peaks provided by Fig. 5 represents the modes involve in the interference and the typically FP response is modified, this will be demonstrated in Section 3 when physical parameter modifies the optical path into the structure. Nonetheless, this response can be expressed by [12]

$$I_T = \sum_{a=1}^{n} I_a + \sum_{a=1}^{n} \sum_{b=1}^{m} \sqrt{I_a I_b} \cos(\Delta\phi_{ab}). \quad (1)$$

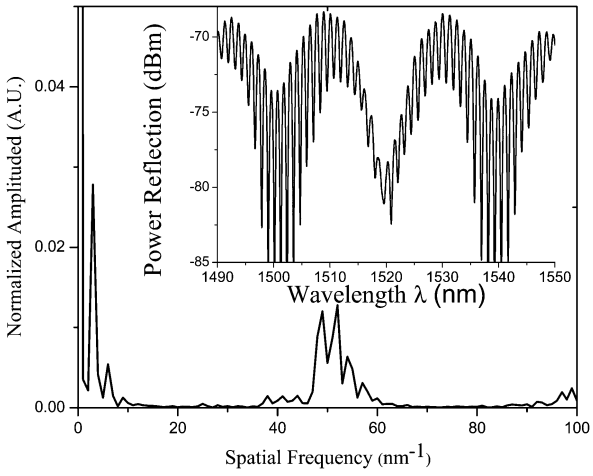

Fig. 5. Spatial frequency analysis.

Here, I_a and I_b represent the intensity of the core and cladding modes that generated the interference spectrum and $\Delta\phi_{ab}$ represents the phase between the modes involve. In this structure four different phase changes will occur. The first phase change between the modes involve is provided by C_1 and can be expressed by $\Delta\phi_{ab_1} = 4\pi n_{c_1} l_{c_1}/\lambda$, where n_{c_1} is the refractive index of the air cavity $(n_a = 1.00)$, l_{c_1} represents the cavity distance and λ is the wavelength of the light in the cavity, this parameter (λ) will remains constant in all the phase changes. The next phase change at C_2 is related with two different optical paths as was explained above, because of that, this one can be expressed by $\Delta\phi_{ab_2} = 2\pi(n_{Core\_C_2} - n_{Cladding\_C_2})l_{C_2}/\lambda$, here $(n_{Core\_C_2} - n_{Cladding\_C_2})$ is the effective refractive index difference between the modes involve in the cavity and l_{C_2} is the cavity distance. C_3 provided the third phase change, $\Delta\phi_{ab_3} = 2\pi n_{C_3} l_{C_3}/\lambda$, where n_{C_3} and l_{C_3} are the air cavity refractive index and the cavity length. Finally, the last phase change occurs at C_4 and can be expressed by $\Delta\phi_{ab_4} = 2\pi n_{C_4} l_{C_4}/\lambda$, here n_{C_3} and l_{C_3} are the silica cavity refractive index and the cavity length. All these phases change govern the structure when physical parameter modifies the optical paths in the cavities and the response will be different than conventional FP cavity response. Moreover, the fringe contrast (V) can be modified by the interaction between the fundamental mode and the predominant high order mode by the relation

$$V = -10\log_{10}\left[\frac{1 - 2\left(\frac{I_b}{I_a}\right)^{\frac{1}{2}}}{1 + \left(\frac{I_b}{I_a}\right)}\right]. \tag{2}$$

3. Refractive Index, Load, and Temperature Response

As has been probed, this kind of all fiber structures has a good performance in refractive index (RI) and load detection. However most of the all fiber FP cavities are phase-temperature independent, due to the thermal silica properties. Nevertheless in this modified FP structure, C_2 provided a phase delay that can be sensitive to thermal, RI and load effects and generated a different response than conventional FP cavity, in order to probe this modified response, some experiments were carried out into a temperature room.

3.1. Response to Refractive Index

With the purpose to characterized the response of the MIFPI to RI changes and propose a detection system, the experimental setup implemented in Fig. 2 was used, here the MIFPI was immersed into a water-glycerol concentrations, these mixtures provided a refractive index variation that can be approximated by [17]. The response of the MIFPI under different RI variation at specific wavelength range is shown in Fig. 6.

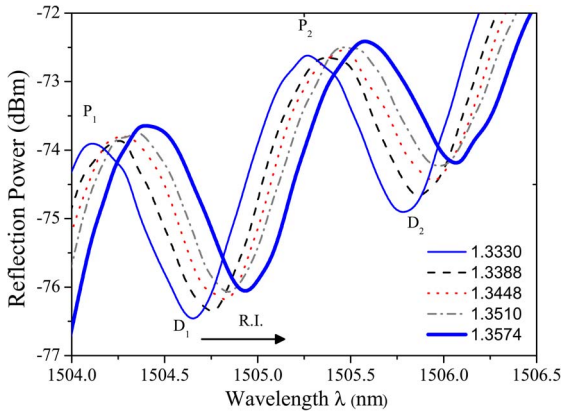

Fig. 6. MIFPI interference spectrum for different RI estimated values.

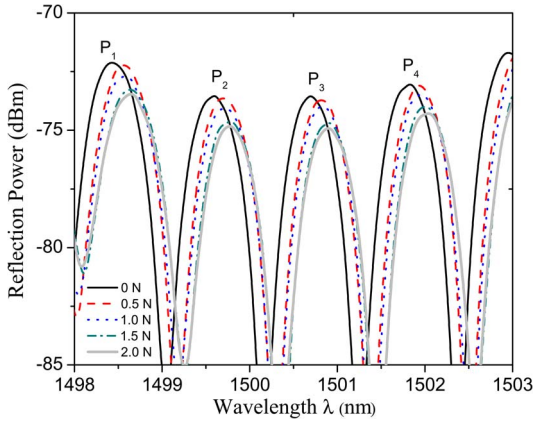

Fig. 7. Load response at specific wavelength range.

As it can be observed in Fig. 6, uniform wavelength shifting is exhibit in the MIFPI interference pattern when refractive index is applied from 1.3330 to 1.3574. However, it is important to point out that usually external refractive index applied around FP cavities provided an intensity modulation. Nevertheless, the wavelength shifting in this analysis has to do with the phase delay provided by cavity C_2, here when the light that travels into the sort of cladding between C_1 and C_3, a phase delay occur by refractive index difference (Δn) between the refractive index of the sort of cladding in cavity C_2 $(n_{Cladding\_C_2})$ and the external refractive index applied $(n_{External})$, when $n_{External}$ is increased the $\Delta\phi_{ab_2}$ change and the wavelength shifting occur; moreover, at the same time small intensity modulation can be appreciated as a result of the reflection modification by the $n_{External}$ at the tip cavities. In order to estimated the sensitivity (D_1) was chosen for simplicity. Here the MIFPI showed to sensitivity around 11 nm/RIU and using a typical OSA resolution (0.001 nm) good sensitivity around $9.1 * 10^{-5}$ RIU is presented. This sensitivity can be compared with some prior works.

3.2. Load Detection

In order to study load effects over the all fiber structure proposed; the MIFPI was set between two small and thin glass layers and using the schematic configuration showed in Fig. 2 the load effect over the MIFPI was monitored. Here small load variation was analyzed (0.5 N), this load were distributed over all the MIFPI structure. Generally, the FP cavity provided a wavelength shift due to the load modifies the shape of the cavity. However, in Fig. 7, the interference power decrease as can be appreciated. This is related with the losses at the interfaces $C_1 - C_2$ and

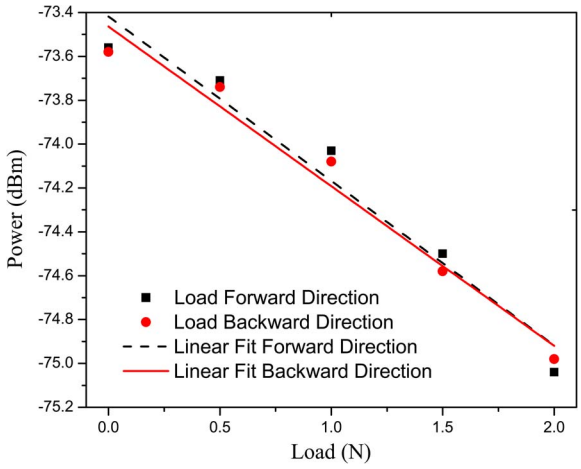

Fig. 8. Linear response for load applied at 1500 wavelength centered.

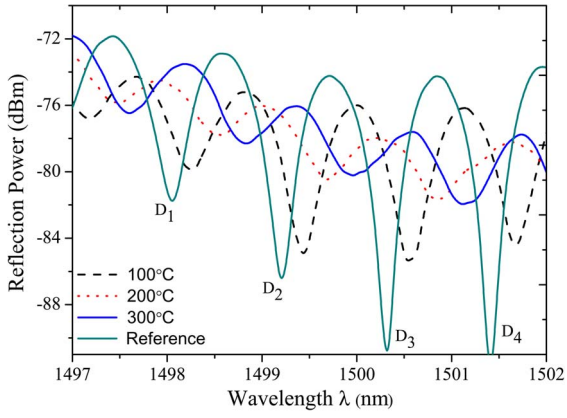

Fig. 9. Collected temperature spectral of MIFPI.

$C_2 - C_3$ when the load is applied, moreover, the predominant high order mode suffers a decrement, which will affect the fringe constant [see (2)]. The small wavelength shift presented in Fig. 7 when the load is applied has to do with small FP cavities deformations.

To analyze the sensitivity, P_3 was chosen arbitrary and 0.75 dB/N was obtained, moreover resolution around $1.33 * 10^{-3}$ N it can be estimated. The response when the load is applied in forward and backward direction at P_3 (1500.8 nm), can be observed in Fig. 8 and the lack of hysteresis is exhibits. This analysis presents a linear response that can be used to propose an easy and controllable intensity modulated fiber optic sensor for small load detection.

3.3. Temperature Analysis

In previous works, has been reported that for specific temperature range all-fiber FP interferometers are immune to thermal effects, this advantage allow to operated for a specific physical parameter without noise. To analyze temperature effects over MIFPI, the experimental setup in Fig. 2 was used and the MIFPI was set over a controllable hotplate. Temperature variations from temperature room to 300°C were applied. Here, the fringe contrast interference decreases when the temperature increases as can be appreciated in Fig. 9.

However, when the fringe contrast decrease, ambiguity temperature detection can be presented, because of that D_2 was chosen arbitrary to study the sensitivity, due to a clear wavelength shift is presented, and $3.66 * 10^{-3}$ nm/°C is estimated. Besides, using the minimal

resolution provided by the OSA, during this analysis (0.002 nm), a resolution of 5 °C can be expected. The temperature response is related with a change in the optical path into all the cavities. As is well known to generate a change length into the MIFPI, higher temperature value need to used. Nevertheless, the change expressed here refers to an effective refractive index change that the predominant high order mode experiments when the temperature increases. The wavelength shifts presented in the analyses carry out in this work are related with the effective refractive index change Δn, which is directly related with $\Delta\phi$ from (1). Moreover, the fringe contrast variations presented in the experiments has to do with (2), and the high order mode (I_2) decrement. According to the results showed for the parameters studied in this work it can be said that MIFPI is more sensitive to temperature changes, due to fringe contrast variation as well as wavelength shifting is present, this can be an undesirable effect and generate ambiguity detection when two parameters presented in the system need to be analyzed; however, a low cost post processing technique proposed by [18] can be implemented to eliminate this issue.

4. Conclusion

In this work, Modified Intrinsic Fabry–Perot Interferometer (MIFPI) by versatile technique has been proposed. Besides, refractive index, temperature and load response were demonstrated. The MIFPI is composed by several FP cavities that were formed using splicer discharges over SMF28-HC-1060 splice joint. This all fiber structure exhibits a free spectral range $(\Delta\lambda)$ around 1.5 nm as well as a fringe contrast (V) variation generated by the wavelength cavity losses dependence that affect the fundamental mode and high order mode interaction. The all fiber structure showed in this work, allows us to detect small refractive index variations from 1.3330–1.3574 and a resolution around $9.1 * 10^{-5}$ RIU was obtained by phase modulation. Load detection was carrying out and resolution of $1.33 * 10^{-3}$ N by intensity modulation was achieved. In the last experiment, temperature was applied over the MIFPI and resolution close to 5 °C was estimated by wavelength shifting. The cavity C_2 in the structure provided a modified response expected in all-fiber FP cavities, and by the use of this cavity, sensitivity can be modified. The structure presents a low cost fabrication and robustness and can be implemented according to the field reach demands. Moreover, as a result of the phase modulation exhibited by the MIFPI when a physical parameter is applied and its small free spectral range $(\Delta\lambda)$, in future work, the application of this all fiber structure in a cavity fiber laser will be analyzed.

Acknowledgment

In memory of my parents: Julian Estudillo-Ruiz and Obdulia Ayala-Martinez.

References

[1] M. Islam, M. Ali, M.-H. Lai, K.-S. Lim, and H. Ahmad, "Chronology of Fabry–Perot interferometer fiber-optic sensors and their applications: A review," *Sensors*, vol. 14, no. 4, pp. 7451–7488, Apr. 2014.
[2] H. Y. Choi, G. Mudhana, K. S. Park, U.-C. Paek, and B. H. Lee, "Cross-talk free and ultra-compact fiber optic sensor for simultaneous measurement of temperature and refractive index," *Opt. Exp.*, vol. 18, no. 1, pp. 141–149, Jan. 2010.
[3] W. Tingting, W. Ming, and N. Haibin, "Micro-Fabry–Perot interferometer with high contrast based on an in-fiber ellipsoidal cavity," *IEEE Photon. Technol. Lett.*, vol. 24, no. 11, pp. 948–950, Jun. 2012.
[4] Z. L. Ran, Y. J. Rao, W. J. Liu, X. Liao, and K. S. Chiang, "Laser-micromachined Fabry–Perot optical fiber tip sensor for high-resolution temperature-independent measurement of refractive index," *Opt. Exp.*, vol. 16, no. 3, pp. 2252–2263, Feb. 2008.
[5] B. Dong, J. Hao, T. Zhang, and J. L. Lim, "High sensitive fiber-optic liquid refractive index tip sensor based on a simple inline hollow glass micro-sphere," *Sens. Actuators B, Chem.*, vol. 171/172, pp. 405–408, Aug./Sep. 2012.
[6] D. Jauregui-Vazquez *et al.*, "Highly sensitive curvature and displacement sensing setup based on an all fiber micro Fabry–Perot interferometer," *Opt. Commun.*, vol. 308, pp. 289–292, Nov. 2013.
[7] O. Ki Dong, J. Ranade, V. Arya, W. Anbo, and R. O. Claus, "Optical fiber Fabry–Perot interferometric sensor for magnetic field measurement," *IEEE Photon. Technol. Lett.*, vol. 9, no. 6, pp. 797–799, Jun. 1997.
[8] D.-W. Duan, Y.-J. Rao, Y.-S. Hou, and T. Zhu, "Microbubble based fiber-optic Fabry–Perot interferometer formed by fusion splicing single-mode fibers for strain measurement," *Appl. Opt.*, vol. 51, no. 8, pp. 1033–1036, Mar. 2012.
[9] J. Ma, J. Ju, L. Jin, W. Jin, and D. Wang, "Fiber-tip micro-cavity for temperature and transverse load sensing," *Opt. Exp.*, vol. 19, no. 13, pp. 12 418–12 426, Jun. 2011.

[10] M. Jun, J. Jian, J. Long, and J. Wei, "A compact fiber-tip micro-cavity sensor for high-pressure measurement," *IEEE Photon. Technol. Lett.*, vol. 23, no. 21, pp. 1561–1563, Nov. 2011.
[11] X. Tan, Y. Geng, X. Li, R. Gao, and Z. Yin, "High temperature microstructured fiber sensor based on a partial-reflection-enabled intrinsic Fabry–Perot interferometer," *Appl. Opt.*, vol. 52, no. 34, pp. 8195–8198, Dec. 2013.
[12] A. Zhou *et al.*, "Hybrid structured fiber-optic Fabry–Perot interferometer for simultaneous measurement of strain and temperature," *Opt. Lett.*, vol. 39, no. 18, pp. 5267–5270, Sep. 2014.
[13] M. S. Ferreira *et al.*, "Post-processing of Fabry–Perot microcavity tip sensor," *IEEE Photon. Technol. Lett.*, vol. 25, no. 16, pp. 1593–1596, Aug. 2013.
[14] S. Liu *et al.*, "High-sensitivity strain sensor based on in-fiber improved Fabry–Perot interferometer," *Opt. Lett.*, vol. 39, no. 7, pp. 2121–2124, Apr. 2014.
[15] D. Jauregui-Vazquez *et al.*, "An all fiber intrinsic Fabry–Perot interferometer based on an air-microcavity," *Sensors*, vol. 13, no. 5, pp. 6355–6364, May 2013.
[16] J. C. Hernandez-Garcia *et al.*, "Generation of a spectrum with high flatness and high bandwidth in a short length of telecom fiber using microchip laser," *Opt. Commun.*, vol. 292, pp. 126–130, Apr. 2013.
[17] G. P. Association, *Physical Properties of Glycerine and Its Solutions*. New York, NY, USA: Glycerine Producers' Assoc., 1963.
[18] D. Jauregui-Vazquez *et al.*, "Bitapered fiber sensor: Signal analysis," *Sens. Actuators B, Chem.*, vol. 218, pp. 105–110, Oct. 2015.